



**HAL**  
open science

## Measurement and modelling of high resolution flow-velocity data under simulated rainfall on a low-slope sandy soil

Lucile Tatard, Olivier Planchon, John Wainwright, Guillaume Nord, David Favis-Mortlock, Norbert Silvera, Olivier Ribolzi, Michel Esteves, Chi Hua Huang

### ► To cite this version:

Lucile Tatard, Olivier Planchon, John Wainwright, Guillaume Nord, David Favis-Mortlock, et al.. Measurement and modelling of high resolution flow-velocity data under simulated rainfall on a low-slope sandy soil. *Journal of Hydrology*, 2008, 348 (1-2), pp.1-12. ird-00268400

**HAL Id: ird-00268400**

**<https://ird.hal.science/ird-00268400>**

Submitted on 1 Apr 2008

**HAL** is a multi-disciplinary open access archive for the deposit and dissemination of scientific research documents, whether they are published or not. The documents may come from teaching and research institutions in France or abroad, or from public or private research centers.

L'archive ouverte pluridisciplinaire **HAL**, est destinée au dépôt et à la diffusion de documents scientifiques de niveau recherche, publiés ou non, émanant des établissements d'enseignement et de recherche français ou étrangers, des laboratoires publics ou privés.

# Measurement and modelling of high resolution flow-velocity data under simulated rainfall on a low-slope sandy soil

L. Tatar<sup>1)</sup>, O. Planchon<sup>2)</sup>, J. Wainwright<sup>3)</sup>, G. Nord<sup>4)</sup>, D. Favis-Mortlock<sup>5)</sup>, N. Silvera<sup>2)</sup>, O. Ribolzi<sup>6)</sup>, M. Esteves<sup>4)</sup>, Chi Hua Huang<sup>7)</sup>

<sup>1</sup>. LGIT, Université Joseph Fourier, Maison des Géosciences, 1381 rue de la Piscine – Domaine Universitaire – 38400 Saint-Martin-d’Hères, France. ltatard@obs.ujf-grenoble.fr

<sup>2</sup>. Institut de Recherche pour le Développement (IRD), Po Box 1025 Kasetsart University. 10903 Bangkok.

<sup>3</sup>. Sheffield Centre for International Drylands Research, Department of Geography, University of Sheffield, Winter Street, Sheffield, S10 2TN, UK.

<sup>4</sup>. LTHE, Université Joseph Fourier, 1025 rue de la Piscine –Domaine Universitaire – 38400 Saint-Martin-d’Hères, France.

<sup>5</sup>. School of Geography, Queen's University Belfast, Belfast, UK.

<sup>6</sup>. Institut de Recherche pour le Développement (IRD), Vientiane, Lao PDR.

<sup>7</sup>. NSERL, 1196 Building SOIL, Purdue University, West Lafayette, IN 47907-1196, USA.

## Abstract

The study presented here is focussed on the question of the hydraulic nature of the threshold that allows a rill to start. A rainfall-simulation experiment was carried out to produce high-resolution flow-velocity data. The experiment employed a 10 m × 4 m experimental plot with a 1 % slope, which had been previously eroded and had a small rill formed in the middle. The experiment consisted of a 2 h 15’-long rainfall at a constant intensity of 69 mm h<sup>-1</sup>. Surface elevation was measured before rainfall at a horizontal resolution of 2.5 cm across, and 5 cm along the slope direction. During rainfall, flow velocities were measured at 68 locations on the plot with the Salt Velocity Gauge technology, an automated, miniaturized device based on the inverse modelling of the propagation of a salt plume. The experiment led to the collection of flow-velocity measurements which are novel in three ways: (i) the small size of the measured section, which was only 10-cm long and 1-cm wide, (ii) the wide range of measured flow velocities, which ranged from 0.006 m s<sup>-1</sup> to 0.27 m s<sup>-1</sup> and, (iii) the large number of measured locations.

The flow-velocity field was simulated with three models: PSEM\_2D solves the Saint-Venant equations in 2D, MAHLERAN uses a 1D kinematic wave in the slope direction coupled with a 2D flow-routing algorithm, and Rillgrow2, which involves an empirical runoff algorithm that is close in principle to the diffusion-wave equation in 2D. The Darcy-Weisbach friction factor ( $ff$ ) and the infiltration parameters were calibrated in all cases to investigate the capabilities of the different models to reproduce flow hydraulics compatible with the onset of rilling. In a first

1 set of numerical experiments,  $ff$  was set uniform, and calibration used only the hydrograph. The  
2 comparison of simulated and observed flow-velocity field showed that PSEM\_2D was the  
3 most satisfying model, at the cost of longer computational time. MAHLERAN gave  
4 surprisingly good results with regards to the simplicity of the model and its low computational  
5 needs. However, all models largely underestimated the highest velocity values, located in the  
6 rill. Furthermore, none of the models was able to simulate the Reynolds ( $Re$ ) and Froude ( $Fr$ )  
7 numbers. The next numerical experiment was done with PSEM\_2D. Non-uniform  $ff$  values  
8 were calibrated by fitting the simulated flow-velocity field to the observed one. The latter  
9 simulation produced realistic simulations of  $Re$  and  $Fr$ . The hydraulic conditions at the  
10 transition from interrill flow to rill flow are discussed. The results support the theory that  
11 supercritical flows are a necessary condition for a rill to emerge from a smooth surface.

12

13 *Key words:* rainfall simulation, water erosion, erosion models, rill, interrill, Senegal

14

## 15 **Introduction**

16 Rill erosion is a major contributor to sediment removal from agricultural fields. Recent studies  
17 based on rare earth elements have shown experimentally that rill erosion can produce 4.3 to 5  
18 times (Song et al., 2003) and even 29 times (Whiting et al., 2001) as much sediment as interrill  
19 erosion. Even on small plots ( $1.5 \times 3$  m), Yang et al. (2006) showed that simulated rainfall at  
20 an intensity of  $73 \text{ mm h}^{-1}$  can cause twice as much rill erosion as interrill erosion after only  
21 13 min of runoff. The onset of rills, and the development of the rill pattern, can even be the key  
22 process that explains erosion on the most severe events. Cerdan et al. (2002), for example,  
23 reported  $10 \text{ t ha}^{-1}$  of rill and gully erosion in a single month in a 94-ha catchment in Normandy  
24 (France) during the dramatic winter of 1999, while water erosion in the region is normally  
25 dominated by interrill processes. However and despite these observations, the dynamics of rill  
26 patterns, and the onset of rilling, are not taken into account in most soil-erosion models, with  
27 the noticeable exception of experimental models, such as RillGrow (Favis-Mortlock, 1998) or  
28 novel models in their preliminary versions, such as PSEM\_2D (Nord and Esteves, 2005) or  
29 MAHLERAN (Wainwright et al., *in review*). The WEPP model, described by Gilley et al.  
30 (1988), for example, assumes the rill density is one rill per metre transversally to the slope. In  
31 the LISEM model (de Roo et al., 1996) all erosion is assumed to be rill erosion, although rills  
32 are not explicitly simulated. During rainfall, such models are unable neither to modify the rill  
33 density nor to simulate its dynamics.

34 After they have developed in the landscape however, rill networks have been thoroughly  
35 described, and their density related to landscape properties (Patton and Schumm, 1975; Parsons  
36 1987; Thorne and Zevenbergen, 1990; Montgomery and Dietrich, 1992; Vandaele et al., 1996;  
37 Desmet and Govers, 1997; Desmet et al., 1999). Experimental studies have been devoted to rill  
38 density, either in field such as in Mancilla et al. (2005) or laboratory experiments (Gómez et  
39 al., 2003; Rieke-Zap and Nearing, 2005; Darboux and Huang, 2005). Flow characteristics in  
40 rills have also received considerable attention (Govers, 1992; Abrahams et al., 1996; Nearing

1 et al., 1997, Gimenez and Govers, 2001). It has even proved possible in some cases, like  
2 Chaplot et al. (2005), to simulate rill development numerically during chosen storm events that  
3 are already known to have caused rill erosion.

4 However, the dynamics of rilling is poorly known, since most field work, such as Desmet et al.  
5 (1999) or Chaplot et al. (2005), refer to rill descriptions made after rainfall, with no  
6 information about the onset and development of rills. As a consequence of the lack of  
7 information about the onset and development of rills, currently existing distributed erosion  
8 models are unable to predict whether rilling and gullyng will occur or not during a given storm  
9 event. This is one of the acknowledged causes of their poor predictive capabilities reported by  
10 Jetten et al. (1999), whose conclusions are rewritten more abruptly in Jetten et al. (2003). A  
11 fundamental part of this problem is the ability of models to represent the processes at work in  
12 the landscape. At the transition from interrill flow to rill flow, these processes are critically  
13 represented by hydraulic properties of the flow. However, little attention has been paid in the  
14 literature to the ability of models to reproduce the specific hydraulic conditions at this  
15 transition.

16 The study presented here is therefore focussed on the question of the hydraulic nature of the  
17 threshold that allows a rill to start. A rainfall-simulation experiment was carried out to address  
18 this question. The experiment took place at Thies, Senegal, on a 40-m<sup>2</sup> plot with a sandy soil  
19 and low slope (1%). Flow velocity was measured at 68 individual points on the plot with a  
20 miniaturized version of the salt velocity gauge (SVG) technology described by Planchon et al.  
21 (2005). SVG is an automated salt-tracing technique which provides reliable velocity data over  
22 a wide range of flow speeds and with no lower limit on flow depth. The apparatus specifically  
23 designed for this experiment allowed the flow velocity to be measured at a high resolution,  
24 averaging over 10-cm long by 1-cm wide sections of the flow.

25 Three existing models of different levels of complexity have been used, in order to test their  
26 ability to simulate the high resolution data made available by the SVG technology. The use of  
27 several models was expected to bring some insights about the research needs for the modelling  
28 of rill initiation and rill flow. At the same time, the study of the onset of rilling was expected to  
29 benefit from the variety of models used, especially if some common result was produced.

30 The question of the hydraulic nature of the threshold that allows a rill to start is directly related  
31 to the interactions between roughness and flow conditions. These interactions are potentially  
32 complex, especially in the presence of stones or vegetation, as reported by Abrahams et al.  
33 (1995). In such a case, the Darcy-Weisbach friction factor,  $ff$ , may increase or decrease with  
34 increasing Reynolds number,  $Re$ , depending of a number of other parameters such as flow  
35 depth and the nature of obstacles, as investigated experimentally by Järvelä (2002). In the  
36 absence of these complex conditions, the interaction between roughness and flow falls into two  
37 distinct categories.

38 First, laminar flows have decreasing values of  $ff$  with increasing  $Re$  in all cases, as reported by  
39 Dunkerley et al. (2001). Nearing et al. (1997) have also reported decreasing  $ff$  with increasing  
40  $Re$  for  $Re$  values up to 70,000 in a flume experiment carried on pure sorted quartz sand. The

1 common characteristic to the two abovementioned experiments was the inability of the flow to  
2 significantly modify the soil roughness, either because of lack of available power in the  
3 laminar case, or because of specific precautions in the experimental design in the experiment of  
4 [Nearing et al. \(1997\)](#).

5 Secondly, in turbulent conditions, when strong feedback interactions allow the flow conditions  
6 to modify the bed roughness,  $ff$  is found to increase with increasing  $Re$  ([Nearing et al., 1997](#);  
7 [Hessel et al., 2003](#)). Such feedback interactions were first described by [Govers \(1992\)](#), who  
8 showed that flow velocity in eroding rills is independent of the slope angle. This situation  
9 forms the second kind of interactions mentioned above, which involves the Froude number  $Fr$ .  
10 [Grant \(1997\)](#) hypothesized that in flows with mobile beds,  $Fr$  could not be higher than unity  
11 over long distances or long periods of time. [Gimenez et al. \(2004\)](#) investigated experimentally  
12 the reasons for such a limitation. They produced the following hypotheses: (i) critical flow was  
13 a necessary condition for rill initiation, and (ii) interaction with  $Fr$  is related to the  
14 development of small hydraulic jumps along the rill. In the light of the experiment of [Gimenez](#)  
15 [et al. \(2004\)](#), the role of  $Fr$  in the feedback between flow conditions and bed roughness can be  
16 explained as follows: when the flow is accelerating in a rill due to gravity, it finally reaches  
17 supercritical velocity. At supercritical velocities, any tiny change in the channel geometry  
18 (which obviously are many in a natural channel) will potentially generate a small hydraulic  
19 jump. The jump has two connected consequences: (1) by definition, the jump changes the flow  
20 conditions from supercritical to subcritical, thus preventing any eroding rill to sustain  
21 supercritical speed over long distances, and (2) the high turbulence associated with the jump  
22 results in eroding the channel at the jump location, thus enlarging the tiny irregularity that  
23 initially caused the jump. If this scenario is correct, supercritical velocity should be a necessary  
24 condition for a rill to emerge from a smooth surface. Investigating this hypothesis derived from  
25 the work of [Gimenez et al. \(2004\)](#) was thus a further objective of this experiment.

## 28 **Material and methods**

### 29 *The new generation of SVG*

30 The SVG technology has been presented in [Planchon et al. \(2005\)](#). It consists of injecting salty  
31 brine into the flow and recording the conductivity peak simultaneously at two locations  
32 downstream separated by a known distance of a few centimeters. The flow velocity is  
33 calculated by inverse modelling of the propagation of the conductivity peak between the two  
34 probes. The model used is a 1D convection-dispersion model (Eq. 1). [Hayami \(1951\)](#) cited by  
35 [Henderson \(1966\)](#), gave Eq. 2 as the solution of Eq. 1 when  $C(0, t)$  is the Dirac function, *i.e.*  
36 injection is instantaneous. Eq. 3 describes the least-squares sum that is minimized in the model  
37 used by the SVG.

$$\frac{\partial C}{\partial t} = -u \frac{\partial C}{\partial x} + D \frac{\partial^2 C}{\partial x^2} \quad (1)$$

1

$$C = \frac{x}{2\sqrt{\pi \cdot D \cdot t^3}} \exp\left(-\frac{(u \cdot t - x)^2}{4D \cdot t}\right) \quad (2)$$

2 Where  $C$  is salt concentration ( $\text{g l}^{-1}$ );  $t$  is time (s);  $x$  is the distance to the injection point (m);  $u$   
3 is flow velocity ( $\text{m s}^{-1}$ );  $D$  is dispersion ( $\text{m}^2 \text{s}^{-1}$ ).  
4

$$ssq = \sum_i \left[ (C_1 \otimes \bar{C}) - (a \cdot C_2 + b) \right]^2 \quad (3)$$

5 Where  $C_1$  and  $C_2$  are salt concentration ( $\text{g l}^{-1}$ ) at the upstream and the downstream probe,  
6 respectively;  $\otimes$  is the convolution product;  $\bar{C}$  is Hayami's solution from Eq. 2 with  $x$  being the  
7 inter-probe distance, i.e. 0.1 m;  $a$  and  $b$  are coefficients that account for salt losses between the  
8 two probes (due to infiltration, lateral dispersion of the brine or other causes);  $ssq$  is the  
9 quadratic sum that is minimized by fitting  $u$ ,  $D$ ,  $a$  and  $b$  for each pair of peaks.

10 The new generation of SVG was operated by two persons. Operator A worked on a bench that  
11 crossed the plot, providing access to the centre of the plot during rainfall without stepping in it.  
12 S/he placed the probes at the measuring locations and injected salty brine a few centimetres  
13 upstream from the probes. The brine was coloured with potassium permanganate to allow for  
14 visual control of the tracing process. Four probes were multiplexed to the datalogger, allowing  
15 four locations to be measured simultaneously. Operator B was at the computer. After operator  
16 A had placed the probes, the data acquisition and the brine injection was simultaneously  
17 triggered at a given signal. The SVG apparatus then acquired salt conductivity data at 200 Hz.  
18 The model described above (Eq. 3) was run at the end of the measurements, and output the  
19 fitted values of the flow velocity, which are hereafter denoted “measured velocity”.

20 Each series of measurement at the multiplexed four locations was repeated three times.  
21 Measured and modelled peaks, as well as the flow velocity, were displayed on the computer in  
22 real time. This procedure allowed operator B to assess the quality of the measurement, and  
23 eventually to request another trial of three replications at the same place. Not more than six  
24 replications were done, even in the case of repeated unsatisfactory results. Whatever the  
25 measurement quality was considered to be in the field, all the measurements were recorded in  
26 the computer together with additional details output by the inverse modelling procedure.

27 This procedure resulted in a total of 348 individual velocity measurements covering 72  
28 different locations. After the experiment, the entire set of recorded data (i.e. disregarding the  
29 initial, subjective, quality assessment done in real time on the field) went through a procedure  
30 that rejected unreliable results. In this procedure, a high degree of confidence in the data used  
31 has been imposed, at the cost of a smaller final dataset. 122 individual measurements, covering  
32 68 locations, have finally been selected by this automatic procedure for further analysis.

33

## 1 *Rainfall-simulation plot*

2 The rainfall-simulation site was located at Thies, Senegal (14°45'43" N, 16°53'16" W). The  
3 plot was 10 m long by 4 m wide, with a 1% slope, and a sandy soil (1% clay, 7% silt, 43% fine  
4 sand, 49% coarse sand). The rainfall simulator was as described by [Esteves et al. \(2000a\)](#). It  
5 allowed for rainfall at a constant average intensity of 69 mm h<sup>-1</sup>; In order to limit wind effects,  
6 which may cause noticeable variations of rainfall intensity, simulations were carried out at a  
7 maximum wind speed of 1 m s<sup>-1</sup>. Six tipping-bucket rain gauges with electronic recording were  
8 placed along the plot borders for monitoring the actual rainfall intensity. The flow discharge  
9 was collected in a trough and alternately directed, via a 10-cm flexible hose, into two 150-litre  
10 cylindrical buckets, one being filled while the other was drained. The volume in the filling  
11 bucket was monitored by electronically recording the rise of a float. The resolution of this  
12 apparatus was 2.5 litres. The typical flow discharge at steady state was 0.5 l s<sup>-1</sup>.

## 13 *Rainfall-simulation experiment*

14 Because the SVG technology did not allow more than four locations to be measured at a time,  
15 the entire set of measurements required more than an hour to complete. Two conditions was  
16 needed to make the measurements as comparable as possible to each other, disregarding the  
17 precise timings of measurements. Condition 1 is a steady-state flow: the velocity measurements  
18 must be carried out at steady rainfall, runoff and infiltration rates. This condition was achieved  
19 by using a 2 h 15'-long continuous rainfall at constant rainfall intensity (69 mm h<sup>-1</sup> on average).  
20 Flow velocity was measured during rainfall, after the flow discharge had stabilized. Condition  
21 2 was a steady flow-pattern: the flow pattern must not vary significantly during the flow  
22 velocity measurement. This condition was achieved by applying rainfall on an already 'old'  
23 surface. In this purpose, the surface was prepared on day 1 of the experiment as follows. First,  
24 a wetting rainfall of 20 mm was applied and the plot was manually ploughed to a depth of  
25 50 cm. The surface was then raked in order to form a slight V shape, with 1% slope  
26 longitudinally and 1% slope towards the median axis of the plot. The purpose of the V shape  
27 was to prevent a rill from forming near to the edge of the plot. Finally a total of six hours of  
28 rainfall have been applied on the plot during days one to five. These rains caused the  
29 longitudinal slope to change from straight to slightly concave (fig. 1), while continuous sand  
30 deposits developed in the concave downstream part.

31 The experiment detailed in this article was held on day 7. Days 6 and 8 were used to carry out  
32 microrelief measurements with an enlarged version of the relief-meter described by [Planchon  
33 et al. \(2001\)](#). It consists of a vertical rod with a sensor at the end that detects the soil surface.  
34 Stepper motors allow the apparatus to move in small increments in all directions. The  
35 horizontal resolution is 2.5 cm transversally to the plot and 5 cm longitudinally. The vertical  
36 precision is 0.5 mm. With a maximum acquisition rate of 1.6 point s<sup>-1</sup>, the 32,000 measured  
37 points of the entire plot required a full working day.

38 At the end of the experiment, a series of digital photographs of the plot were taken from a  
39 height of 6 metres above ground level. The pictures were combined in a single file and  
40 geometrically corrected so that each pixel corresponds to one square millimetre in the field.



1 The resulting image can be combined with a DEM to produce virtual images of the surface.  
2 Fig. 1 shows one of these views with the relief magnified ten times and the colour contrast  
3 enhanced. The native soil appears in black (its natural colour is a yellowish light brown). White  
4 and reddish colours correspond to various types of sand deposits.

5

#### 6 *Hydraulic formulas used*

7 In terms of the flow hydraulics as discussed above, the Reynolds number is defined as:

$$8 \quad Re = 4 u r / \nu \quad (4)$$

9 where  $u$  is average velocity ( $\text{m s}^{-1}$ ),  $r$  is hydraulic radius (m) and  $\nu$  is the fluid kinematic  
10 viscosity ( $\text{m}^2 \text{s}^{-1}$ ). This formula is classically used to estimate  $Re$  in shallow free surface flows;  
11 e.g. [Savat \(1980\)](#), [Gilley et al. \(1990\)](#), [Abrahams et al. \(1995\)](#), [Pilotti and Menduni \(1997\)](#).  
12 The Froude number is:

$$13 \quad Fr = u / \sqrt{g h} \quad (5)$$

14 where  $u$  is average velocity ( $\text{m s}^{-1}$ ),  $g$  is gravitational acceleration ( $\text{m s}^{-2}$ ) and  $h$  is flow depth  
15 (m).

16

#### 17 *The models*

18 Three distributed erosion models have been used.

19 **PSEM 2D**, **Plot Soil-Erosion Model 2D** ([Nord and Esteves, 2005](#); [Esteves et al., 2000b](#)), is a  
20 soil-erosion model dedicated to small experimental plots, typically of less than  $100 \text{ m}^2$ .  
21 Overland flow is described by the depth-averaged two-dimensional unsteady flow equations  
22 commonly referred to as the Saint-Venant equations ([Zhang and Cundy, 1989](#)). The friction  
23 slopes are approximated using the Darcy-Weisbach equation (Eq. 6) derived for uniform steady  
24 flow:

$$25 \quad S_{fx} = ff \frac{u_x^2}{8gh}, S_{fy} = ff \frac{u_y^2}{8gh} \quad (6)$$

26 where  $S_{fx}$  is the friction slope in the  $x$  direction ( $\text{m m}^{-1}$ ),  $S_{fy}$  is the friction slope in the  $y$   
27 direction ( $\text{m m}^{-1}$ ) and  $u_x$  and  $u_y$  are the velocity components in the  $x$  and  $y$  directions,  
28 respectively ( $\text{m s}^{-1}$ ). The Darcy-Weisbach friction factor,  $ff$ , may be spatially variable. The  
29 second-order explicit scheme of [MacCormack \(1969\)](#) is used for solving the overland-flow  
30 equations. Infiltration is computed at each node using a Green-Ampt model ([Green and Ampt,  
31 1911](#)).

32 **MAHLERAN** (**Model for Assessing Hillslope-Landscape Erosion, Runoff And Nutrients**;  
33 [Wainwright et al. \(in review\)](#)) is a flexible model that can be used for experimental plots as  
34 well as small watersheds. The hydrological and hydraulics components of the model are



1 essentially as described in [Parsons et al. \(1997\)](#), [Wainwright et al. \(1999\)](#) and [Wainwright and](#)  
 2 [Parsons \(2002\)](#). The hydraulics consists of solving the kinematic wave equation in 1D along  
 3 the flow direction derived from a DEM which depressions have been previously filled using  
 4 the algorithm from [Planchon and Darboux \(2001\)](#). The kinematic wave simplification uses the  
 5 continuity equation (eq. 7) together with the Darcy-Weisbach equation (eq. 8) in one  
 6 dimension, which provides dynamic feedback between flow and roughness in a more realistic  
 7 way than in typical applications of the kinematic wave ([Scoging, 1992](#)).

$$8 \quad \frac{\partial h}{\partial t} + u \frac{\partial h}{\partial x} = e_x \quad (7)$$

9 where  $e_x$  is rainfall minus infiltration ( $\text{m s}^{-1}$ ):

$$10 \quad u = \sqrt{\frac{8 g h S}{ff}} \quad (8)$$

11 where  $S$  is the slope in the flow direction ( $\text{m m}^{-1}$ ).

12 The numerical scheme used with this model is the Euler simple backward difference from  
 13 [Scoging \(1992\)](#). The flow is routed from each cell to one of the four adjacent cells in a finite  
 14 difference grid using a topographically based algorithm based on the greatest difference in  
 15 altitude of the cells. Overland flow is generated as Hortonian (infiltration excess) runoff by  
 16 determining the difference between the rainfall and infiltration rate or as saturation-excess  
 17 runoff by comparison with a saturated soil-moisture content. Infiltration rate is predicted using  
 18 the Smith-Parlange model with modifications to allow runoff infiltration and temporally  
 19 variable rainfall ([Wainwright and Parsons, 2002](#)).

20 [RillGrow2](#) ([Favis-Mortlock, 1998](#); [Favis-Mortlock et al., 2000](#)) is a model dedicated to the  
 21 numerical simulation of emerging rill patterns. Space is discretized at a very high resolution so  
 22 that any cell is considered to be entirely inside, or entirely outside a rill. Each cell is eroding  
 23 independently to each other. Cells lower while eroding. Eroding cells thus attract more water  
 24 flow, subsequently increasing the erosive power of the rill. Because of its high computational  
 25 needs, applications of RillGrow2 are limited to experimental plots of a few tens of square  
 26 metres.

27 RillGrow2 hydraulics consists of calculating a "potential flow velocity" with a Manning-type  
 28 equation, based on the water depth:

$$29 \quad u_{pot} = w h S_f^n, \quad (9)$$

30 where  $u_{pot}$  is "potential flow velocity" ( $\text{m s}^{-1}$ ),  $w$  is an empirical roughness coefficient,  $S_f$  is the  
 31 hydraulic gradient ( $\text{m m}^{-1}$ ) and  $n=0.5$ .

32 The RillGrow2 numerical scheme is unique in soil-erosion modelling: at each time step, the  
 33 model checks a single cell, chosen at random, and processes it. The check consists of  
 34 calculating  $u_{pot}$  and determining whether outflow is possible from this cell. If so, an outlet cell  
 35 is chosen among eight neighbours according to the steepest descent of the free surface. The

1 required amount of water is then passed from the source cell to the destination cell in order to  
2 level the free surface between the two cells. This procedure is then repeated until all cells have  
3 been chosen at the particular time step.

#### 4 *Data preparation*

5 A raw DEM was calculated with 5-cm cells. RillGrow2, which is specifically designed to use  
6 fine resolution relief data, was the only model able to run the raw DEM. PSEM\_2D needed the  
7 following operations on the DEM before numerical oscillations could be avoided: i)  
8 resampling at 10-cm resolution, ii) smoothing with a Gaussian filter, iii) removing  
9 depressions<sup>1</sup>. MAHLERAN required 50-cm cells to be stable. At this resolution the relief was  
10 fully convergent and the flow was always in the direction of slope, which makes acceptable the  
11 assumptions underlying the resolution of the kinematic wave in 1D along the slope direction.

## 12 **Results and discussion**

### 13 *Field evidence of various flow conditions*

14 Fig. 2 is a detailed view of Fig. 1 seen from downstream. It shows the rill and its left bank. The  
15 original photographs of the plot showed subtle variations of browns. They have been enhanced  
16 for contrast, levels and colour saturation by image processing. The resulting map (Figs 1 and 2)  
17 shows four different surface-feature patterns, which correspond to four different flow  
18 conditions.

19 Location A represents a high point with a convex soil surface. No visible flow occurred there.  
20 High points have the colour of the native soil. Considering that transportation by water is  
21 supposed to remove preferentially the soil organic matter and the finest size fractions, sediment  
22 deposits are expected to have lighter colours, while areas with the colour of the native soil are  
23 likely to be sediment sources.

24 In all attempts to measure flow velocity in locations of type A, the coloured brine was found to  
25 leave the injection point very gradually, thus forming a long, coloured tail. This fate indicates a  
26 vanishingly small flow velocity at the base of the flow, due to strong interaction with the soil-  
27 grain roughness, while the top of the water layer could travel along significant distances. Such  
28 a fate is typical of laminar flows. However, this result does not imply that no turbulence could  
29 agitate the flow, especially because of raindrops which were the main source of water agitation  
30 in these locations. As a result, it was often not possible to carry on SVG measurement in  
31 locations of type A because of insufficient peak sharpness.

32 Location B represents the first visible flow. It is characterized by small undulating furrows,  
33 ~10 mm wide and 2 mm deep. Uneven sand grains could be observed in these tiny channels,  
34 slowly creeping downstream until a raindrop hit them and splashed them away.

---

<sup>1</sup> Neither natural depression nor ponds had developed on the plot during the experiment. However, the raw DEM had some small depressions as the consequence of numerical artefacts, especially in the downstream section of the plot, which was very flat.

1 During SVG measurements, the same "long tailed" plumes as in locations of type A were  
2 observed, indicating high interaction with flow bed, and low or little turbulence besides the  
3 raindrop-related flow agitation.

4 At location C, a well established stream was flowing. The soil surface was covered by a  
5 continuous layer of reddish sand that was slowly creeping downstream.

6 During SVG measurements, the tracer left the injection point in a fraction of a second,  
7 indicating a sharp vertical velocity profile that did not allow the tracer to 'stick' to the soil  
8 surface, as it did in laminar (or at least less turbulent) conditions.

9 Location D was characterized by white sand deposits with crossed wavy features typical to  
10 supercritical flow. The white colour of the sand indicates that the sand grains have been  
11 transported by turbulent flow until all clay and organic particles had detached from the grain  
12 itself. These field observations indicate that the flow was certainly turbulent and supercritical  
13 there. Measured velocities were all above  $0.15 \text{ m.s}^{-1}$ . Table 1 summarizes the qualitative  
14 information detailed above.

#### 15 16 *Qualitative results from the models*

17 Since all infiltration models are known to reproduce well the simple conditions of the  
18 experiment with regard to rainfall and infiltration, and the purpose of the study is to investigate  
19 the reproduction of hydraulics characteristics, each model was calibrated from the hydrograph  
20 in order to remove any variability in the results due to misrepresentation of the infiltration  
21 parameters. SVG measurements were not used during calibration. The infiltration parameters  
22 were calibrated from the total runoff and the steady infiltration rate. The friction factor was  
23 calibrated from the hydrograph rise.

24 The velocity field from PSEM\_2D (fig. 3) is consistent with visual observations. One can  
25 notice for example the location of the predicted maximum velocity. It corresponds to the white  
26 sands at the centre of the plot, which we interpreted as a mark of supercritical flow. The pattern  
27 produced by MAHLERAN is similar to PSEM, with a noticeable loss of precision due to the  
28 coarser grid resolution. RillGrow2 predicts a wide area of high velocity in the bottom part of  
29 the plot which corresponds fairly well to the concave area of reddish sand deposits that can be  
30 seen in figures 1 and 3.

31 The  $Re$  predictions follow approximately the same pattern as the flow velocity. However,  
32 according to the threshold of 2000 commonly used for the transition between laminar and  
33 turbulent flows, the spatial extension of turbulent flow is underestimated with regard to the  
34 results of visual observations reported in the previous section.  $Fr$  is even more problematic  
35 since no pattern at all is predicted by PSEM\_2D or NCF while the pattern predicted by  
36 RillGrow2 is not consistent with the field evidence reported above.

37

## 1 *Comparison of measured and modelled velocity*

2 Fig. 4 shows the modelled velocity compared to the observed ones. All models have a better fit  
3 at low velocities than at higher ones. PSEM\_2D and MAHLERAN slightly overestimate the  
4 low velocity and strongly underestimate the high ones. RillGrow2 simulates very well the  
5 slowest flows (*i.e.*  $u < 0.05 \text{ m s}^{-1}$ ) and underestimates the other cases. Precisely localized  
6 maxima or minima cannot be expected to be reproduced by MAHLERAN since measured  
7 velocities are averaged over  $10 \text{ cm}^2$  while the model results represent a  $0.25 \text{ m}^2$  cell. However,  
8 underestimation of velocity values higher than  $0.1 \text{ m s}^{-1}$  is a common result to all models.  
9 Moreover, the degree of underestimation is similar in all of the models, despite the fact that  
10 their cell sizes differ largely. The working hypothesis for further analysis in this article will  
11 therefore be that the underestimation of velocities higher than  $0.1 \text{ m s}^{-1}$  has a common cause  
12 that is shared by the three models.

13

## 14 *Modelling the interaction between friction factor and flow conditions*

15 Underestimation of flow velocity can be solved by using lower values of  $ff$  at the  
16 corresponding locations. PSEM\_2D allows for spatially non-uniform values of  $ff$  at a high  
17 resolution; it is working at a finer scale and solves the full St Venant equations hence not  
18 limited by the assumptions of the other models. It has therefore been chosen as the best  
19 candidate for validating this approach. The following steps were followed.

20 The first step was to fit the velocity modelled by PSEM\_2D (Fig. 4) to Eq. 10, which describes  
21 empirically the gradually increasing underestimation of modelled velocity.

22

$$23 \quad u_0 = b \cdot u_1^a \quad (10)$$

24

25 where  $a=0.5$ ;  $b=0.28$ ;  $u_0$  is measured velocity and  $u_1$  is the velocity predicted by PSEM\_2D.

26 The second step was to consider the set of equations 10 to 13 for estimating the corrected value  
27 of  $ff$ , hereafter denoted  $ff_1$ , that will solve the bias described by Eq. 10. Eq. 11 states the unit  
28 discharge at a given location will not change after  $ff$  is corrected from  $ff_0$  to  $ff_1$ :

$$29 \quad u_0 \cdot h_0 = u_1 \cdot h_1 \quad (11)$$

30 The Darcy-Weisbach equation before and after correction, are, respectively:

$$31 \quad u_0 = \sqrt{\frac{8gh_0s}{ff_0}} \quad (12)$$

$$32 \quad u_1 = \sqrt{\frac{8gh_1s}{ff_1}} \quad (13)$$

33 The solution to this set of equations is thus:

$$ff_1 = ff_0 \cdot u_0^{\left(\frac{3-\beta}{\alpha}\right)} \cdot b^{\left(\frac{\beta}{\alpha}\right)} \quad (14)$$

where  $ff_0 = 0.26$ , the initial calibrated uniform value of  $ff$  used in the model;  $h_0$  and  $u_0$  are flow depth and flow velocity read at a given cell in the PSEM\_2D results shown in fig. 3 and 4;  $u_1$  is the observed velocity; and  $h_1$  is the corresponding flow depth according to the modelled unit discharge.

$ff_1$  was calculated from Eq. 14 at each cell. The resulting map was then smoothed to prevent the model from generating instabilities. A threshold of  $ff < 2$  was finally applied to account for inconsistent velocities predicted at very small water depths, although the value of this threshold proved to have little influence on the final result.

Fig. 5 shows the resulting maps for  $u$ ,  $Re$  and  $Fr$ . The  $Fr > 1$  limit is in fair agreement with the limits of the white sands that has been interpreted as the mark of supercritical flow. The  $Re > 2000$  limit is wider than in the previous simulation (albeit still limited to the central channel). Fig. 6 shows the graph of modelled vs observed velocity. Results are scattered around the 1:1 line, which is the expected result of the use of Eq. 14. Figures 5 and 6 show that the results with varying  $ff_1$  are far more realistic, and closer to the field observations, than those obtained from homogeneous  $ff$ . Independent data are however lacking to assess the exact meaning of  $ff$  calculated this way, which will therefore be denoted “apparent  $ff$ ” hereafter. The physical significance of apparent  $ff$  values calculated individually for 10-cm cells is also an issue because of inherent scale-dependence in the derivation of roughness coefficients (Müller, 2004).

21

## 22 *Equifinality*

23 It is worth mentioning that the change from calibrated uniform  $ff$  to calibrated non uniform  $ff$   
 24 has not changed the hydrograph, despite this change has led to almost doubling the value of the  
 25 highest simulated velocity. This lack of sensitivity of the hydrograph to the high velocity  
 26 values is probably very common.

27 Similarly to any natural watershed, the plot was divided into two areas: a "slow" one at the  
 28 border, denoted S, which covered 91% of the plot area, and a "fast" one at the centre, denoted  
 29 F, and covering 9% of the plot. Because virtually all water flowing on the plot eventually  
 30 concentrates in F, there is intuitive evidence that the hydrograph is sensitive to any change in  
 31 the flow velocity in F, disregarding its little importance in terms of area. This reasoning has led  
 32 to the widely accepted idea (especially in soil erosion modelling) that flow velocity in F can be  
 33 calibrated from the hydrograph. Our experiment has shown that this procedure can produce  
 34 unreliable results in many cases.

35 On the plot, F can be defined as the area where  $u > 0.1 \text{ m s}^{-1}$ . The average fate of a raindrop  
 36 falling at the surface of the plot and flowing downstream has been calculated from the flow-  
 37 velocity field output by PSEM\_2D. This imaginary raindrop spent  $t_{s+f} = 66 \text{ s}$  on the plot,  
 38 divided in  $t_s = 41 \text{ s}$  spent in S and  $t_f = 25 \text{ s}$  spent in F. As a result of the longer time spent at

1 low speed, a change of 1% in the flow velocity in S results in a change of 0.62% in  $t_{s+f}$  while  
2 the same change in F results only in a 0.38% change in  $t_{s+f}$ . Velocity faster than  $0.1 \text{ m s}^{-1}$ ,  
3 which are of crucial importance to soil erosion, had even less influence on the hydrograph: the  
4 same 1% change in velocity values higher than 0.15 and  $0.2 \text{ m s}^{-1}$  produced, respectively, a  
5 change of 0.28% and 0.08% in the average time to the outlet.

6 In brief, using calibrated values of  $ff$  in a soil-erosion model is likely to provide the most  
7 reliable velocity values at low speed, where no erosion occurs, at the cost of potentially large  
8 errors on the flow velocity at the eroding places.

### 9 10 *ff-Re relationship*

11 Fig. 7 shows a log-log plot of the relationship between apparent  $ff$  and  $Re$ . It shows that  
12 apparent  $ff$  was high at low Reynolds numbers and decreased with increasing  $Re$ . This  
13 relationship is consistent with observations from [Nearing et al. \(1997\)](#) as well as [Dunkerley et al. \(2001\)](#),  
14 which fall in the case of no backward interaction of flow conditions to the bed  
15 roughness and roughness elements are small with regard to flow depth, both conditions being  
16 the case in our experiment. Fig. 8 compares our results to those from [Nearing et al. \(1997\)](#).  
17 Each line was drawn within the data limits of the corresponding experiment. It appears that our  
18 results are in continuity to those from [Nearing et al. \(1997\)](#). However, in our experiment, the  
19 dependency of  $ff$  on  $Re$  is weaker than in the study from [Nearing et al. \(1997\)](#). It is likely that  
20 the calibrated, apparent  $ff$  incorporates more than the strict relationship of the flow to the soil  
21 roughness. In particular, some scale effect linked to the cell size must be expected. Additional  
22 experiments in various conditions of flow and slope would probably allow a better  
23 understanding of the reasons of the differences between the two studies.

### 24 25 *Onset of rilling*

26 In this work, we have calculated apparent  $ff$  values in order to allow PSEM\_2D to reproduce  
27 the flow velocity at the 68 measured locations. The resulting modelled velocity field was found  
28 to be consistent with field evidences of supercritical flow within the central channel, and  
29 reasonably consistent with field evidence of turbulent flow in all channels, i.e. the central one  
30 and its principal tributaries. The field evidence gives a high degree of confidence to the  
31 simulated values of flow velocity as well as the corresponding flow depth.

32 The result supports the hypothesis based on [Gimenez et al. \(2004\)](#) experiment, as discussed in  
33 the introduction. According to this hypothesis, a supercritical flow velocity is a necessary  
34 condition for rills to start. The key point is that supercritical flow allows the formation of small  
35 hydraulic jumps where the development of strong turbulence triggers the erosion of what will  
36 be the rill head.  $Fr$  could therefore be a good candidate to use in models in order to predict the  
37 location and timing of rill onset, and therefore to better predict whether a given storm will  
38 cause significant erosion or not.

1 Our results have also shown that a satisfactory simulation of  $Fr$  must take into account the  
2 interaction between  $Re$  and apparent  $ff$ . While the observed relationship is consistent with the  
3 literature, this relationship is known to exhibit considerable variations with flow conditions, as  
4 well as with the nature and size of roughness elements. More research is needed to investigate  
5 this relationship in more complex situations than the raked, planar, smooth sandy surface used  
6 in this experiment, where grain roughness was dominating the interactions between the flow  
7 and the soil surface.

## 9 **Conclusion**

10 The SVG technology has allowed flow-velocity measurement in a wide range of flow speeds  
11 (from  $0.006 \text{ m.s}^{-1}$  to  $0.27 \text{ m.s}^{-1}$  in this experiment). The use of salty brine as a tracer makes  
12 SVG suitable for measuring very shallow flows. The only limitation was the probe size, which  
13 was 1-cm wide and 10-cm long. Thanks to this technology, we were able to measure velocity  
14 in a wide variety of flow conditions, from unconcentrated to concentrated in a small rill, from  
15 laminar to turbulent, and from subcritical to supercritical. The data obtained have been used to  
16 test three hydrological models (PSEM\_2D, MAHLERAN, and RillGrow2) which were very  
17 different from each other, having only in common the use of a Manning/Darcy-Weisbach-type  
18 hydraulic equation with a constant, homogeneous friction factor. The main results were the  
19 following:

- 20 • PSEM\_2D, MAHLERAN and RillGrow2 to a lesser extent, simulated satisfactorily the  
21 patterns of flow velocity and Reynolds number  $Re$ .
- 22 • The Froude number  $Fr$  was not predicted by any of the three models. Even the general  
23 pattern was missed.
- 24 • Low velocities were overestimated (PSEM\_2D and MAHLERAN). High velocities were  
25 largely underestimated (all models).
- 26 •  $Re$  values estimated by the models are realistic. However, the classical threshold of  $Re=2000$   
27 for the transition between laminar to turbulent flow, would predict laminar flow everywhere  
28 on the plot but in the central channel, while field observations suggested the presence of  
29 turbulence even in the tributaries of the main channel.
- 30 • An apparent friction factor  $ff$  was calculated at each cell in order to fit the modelled velocity  
31 with the whole range of observed values. Running PSEM\_2D with the apparent  $ff$  has  
32 improved the simulation of  $Re$  and  $Fr$  patterns. Moreover, apparent  $ff$  appeared to be related  
33 to  $Re$  via a power law similar to the one observed by [Nearing et al. \(1997\)](#) on sandy bare soil  
34 (albeit the range of  $ff$  and  $Re$  differed in the two studies).

35 These results lead to the following conclusions:

- 36 • The hydrograph alone is an insufficient source of information to calibrate  $ff$  (see also  
37 [Parsons et al., 1994](#)). Other sources of data such as the measured velocity field are therefore



1 highly desirable to calibrate any hydrological model dedicated to be coupled to an erosion  
2 model.

- 3 •  $ff$  decreases with increasing  $Re$ , which we interpreted by the fact that the flow becomes less  
4 sensitive to soil roughness when its turbulence increases. This result supports the  
5 conclusion of [Nearing et al. \(1997\)](#) for sandy bare soils and extends them to lower values of  
6  $Re$  than in their study.
- 7 • The usual procedure in soil-erosion models is the calibration, from the hydrograph, of a  
8 single value of  $ff$  for the whole plot. Our results show that this procedure will correctly  
9 calibrate the friction factor at cells where velocity is low to moderate, which dominate the  
10 hydrological response of the plot. Contrarily, the hydrograph will not be significantly  
11 affected by an even dramatic underestimation of the highest velocity because the  
12 corresponding error in terms of average travel time will be small.
- 13 • Uniform  $ff$  leads to erroneous patterns of  $Fr$ . However, when measured velocities are used  
14 to calibrate non-uniform values of  $ff$ ,  $Fr$  patterns and values are satisfactory. [Gimenez et al.](#)  
15 [\(2004\)](#) have demonstrated the importance of  $Fr$  in the development of rills. Any future  
16 model aimed at simulating rill initiation on the basis of these findings should account for  
17 the  $ff$ - $Re$  relationship in order to have realistic simulations of  $Fr$  for using at predicting rill  
18 initiation.
- 19 • The results support the hypothesis according to which supercritical flow is a necessary  
20 condition to the onset of rilling.

## 23 **Acknowledgements**

24 This work was granted by the RIDES project, an ECCO research program. The experiment was  
25 hosted by the Ecole Nationale Supérieure d'Agriculture (ENSA) of Thies, Senegal. The new  
26 miniaturized version of SVG has been developed in a collaborative project between the Institut  
27 de Recherche pour le Développement (IRD) and the USDA-ARS National Soil Erosion  
28 Laboratory (NSERL). The authors are very thankful to Kokou Abotsi, from IRD Dakar,  
29 Senegal, who has been in charge of the construction, operation and maintenance of the rainfall  
30 simulations facility.

## 1 **References**

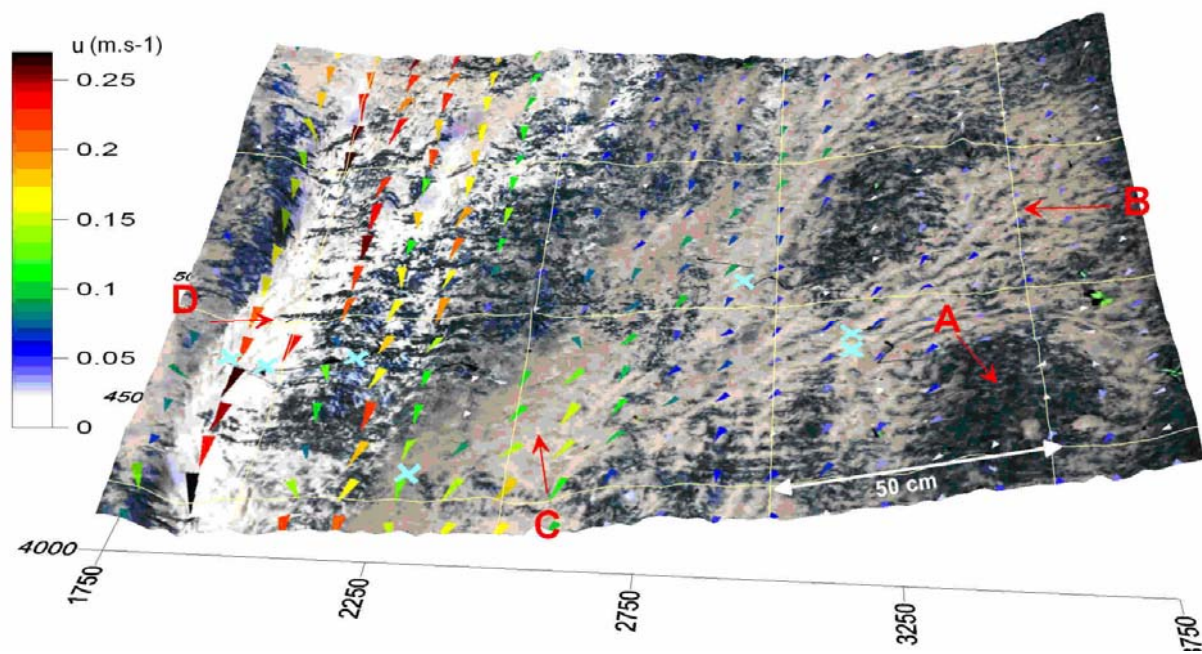
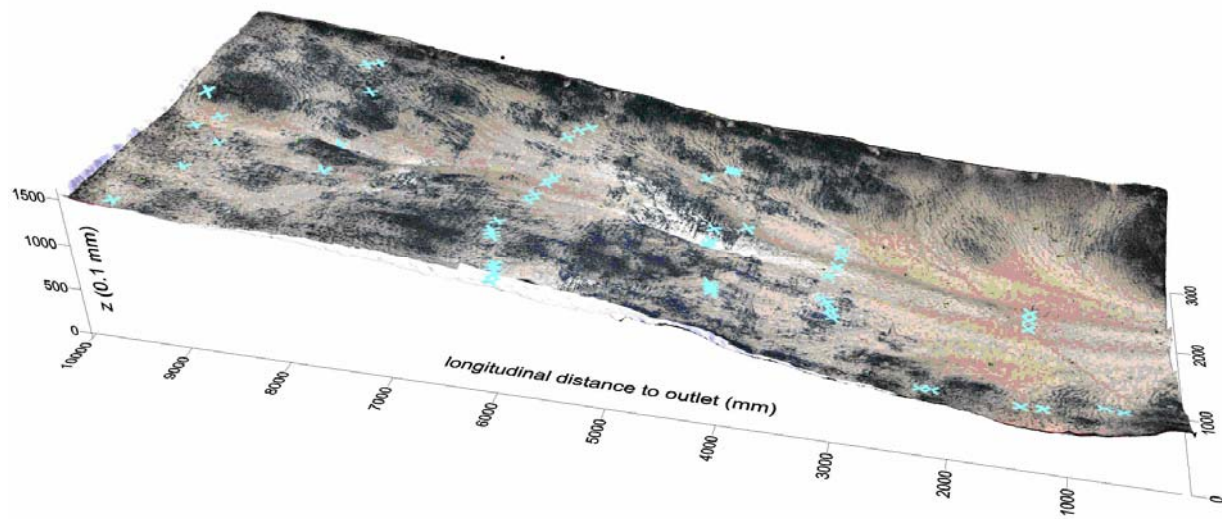
- 2 Abrahams, A.D., Parsons, A.J., Wainwright, J., 1995. Effects of vegetation change on interrill  
3 runoff and erosion, Walnut-Gulch, Southern Arizona. *Geomorphology*, **13**, 37-48.
- 4 Abrahams, A.D., Li, G. and Parsons, A.J., 1996. Rill hydraulics on a semiarid hillslope,  
5 Southern Arizona. *Earth Surface Processes and Landforms*, **21**, 35-47.
- 6 Cerdan, O., Le Bissonnais, Y., Couturier, A., Bourennane H., Souchere V., 2002. Rill erosion  
7 on cultivated hillslopes during two extreme rainfall events in Normandy, France. *Soil and*  
8 *Tillage Research*, **67**(1), 99-108.
- 9 Chaplot, V., Giboire, G., Marchand, P., Valentin C., 2005. Dynamic modelling for linear  
10 erosion initiation and development under climate and land-use changes in northern Laos.  
11 *Catena*, **63** (2-3 Special Issues), 318-328.
- 12 Darboux, F., Huang, C., 2005. Interactions between overland flow and soil surface roughness.  
13 Does soil surface roughness increase or decrease water and particle transfers? *Soil Science*  
14 *Society of America Journal*, **69**(3), 748-756.
- 15 Desmet, P.J.J., Govers, G., 1997. Two-dimensional modelling of the within-field variation in  
16 rill and gully geometry and location related to topography. *Catena*, **29**, 283-306.
- 17 Desmet P.J.J., Poesen, J., Govers, G., Vandaele, K., 1999. Importance of slope gradient and  
18 contributing area for optimal prediction of the initiation and trajectory of ephemeral gullies.  
19 *Catena*, **37**, 377-392.
- 20 Dunkerley, D., Domelow, P., Tooth, D., 2001. Frictional retardation of laminar flow by plant  
21 litter and surface stones on dryland surfaces: A laboratory study. *Water Resources*  
22 *Research*, **37**(5), 1417-1423.
- 23 Esteves, M., Planchon, O., Lapetite, J.M., Silvera, N., Cadet, P., 2000a. The 'EMIRE' large  
24 rainfall simulator: Design and field testing. *Earth Surface Processes and Landforms*, **25**,  
25 681-690.
- 26 Esteves, M., Faucher, X., Galle, S., Vauclin, M., 2000b. Overland flow and infiltration  
27 modelling for small plots during unsteady rain: numerical results versus observed values.  
28 *Journal of Hydrology*, **228**, 265-282.
- 29 Favis-Mortlock, D., 1998. A self-organizing dynamic systems approach to the simulation of rill  
30 initiation and development on hillslopes. *Computers & Geosciences*, **24**(4), 353-372.
- 31 Favis-Mortlock, D.T., Boardman, J., Parsons, A.J. and Lascelles, B., 2000. Emergence and  
32 erosion: a model for rill initiation and development. *Hydrological Processes*, **14**, 2173-  
33 2205.
- 34 Gilley, J. E., Lane, L.J., Laflen, J.M., Nicks, H.D., Rawls, W.J., 1988. USDA-water erosion  
35 prediction project: New generation erosion prediction technology. In: *Modelling*  
36 *Agricultural, Forest, and Rangeland Hydrology*. Symposium Proceedings. Pub.  
37 07-88:260-263. Available from Am. Soc. Agric. Eng., St. Joseph, MI.
- 38 Gilley, J.E., Kottwitz, E.R., Simanton, J.R., 1990. Hydraulic characteristics of rills. *Trans. Am.*  
39 *Soc. Agric. Eng.*, **33**, 1900-1906.
- 40 Gimenez, R., Govers, G., 2001. Interaction between roughness and flow hydraulics in eroding  
41 rills. *Water Resources Research*, **37**, 791-799.

- 1 Gimenez, R., Planchon, O., Silvera, N., Govers, G., 2004. Longitudinal velocity patterns and  
2 bed morphology interaction in a rill. *Earth Surface Processes and Landforms*, **29**, 105-114.
- 3 Gómez J. A., Darboux F., Nearing M.A., 2003. Development and evolution of rill networks  
4 under simulated rainfall. *Water Resources Research*, **39**(6), 1148. doi:  
5 10.1029/2002WR001437
- 6 Govers, G., 1992. Relationship between discharge, velocity and flow area for rills eroding  
7 loose, nonlayered materials. *Earth Surface Processes and Landforms*, **17**, 515-528.
- 8 Grant, G.E., 1997. Critical flow constrains flow hydraulics in mobile-bed streams: A new  
9 hypothesis. *Water Resources Research*, **33**, 349-358.
- 10 Green, W. H., Ampt, G. A. 1911. Studies on soil physics: 1, flow of air and water through  
11 soils. *Journal Agric. Sciences*, **4**, 1-24.
- 12 Hayami S. 1951. On the Propagation of Flood Waves. Disaster Prevention Research Institute,  
13 Kyoto University, Japan, Bulletin no. 1.
- 14 Henderson, FM., 1966. Open Channel Flow. New York: Macmillan Company.
- 15 Hessel, R., Jetten, V., Guanghui, Z. 2003. Estimating Manning's n for steep slopes. *Catena*, **54**,  
16 77-91.
- 17 Järvelä, J., 2002. Flow resistance of flexible and stiff vegetation: a flume study with natural  
18 plants. *Journal of Hydrology* **269**(1-2), 44-54.
- 19 Jetten, V., de Roo, A., Favis-Mortlock, D., 1999. Evaluation of field-scale and catchment-scale  
20 soil erosion models. *Catena*, **37**(3-4), 521-541.
- 21 Jetten, V., Govers, G., Hessel, R., 2003. Erosion models: quality of spatial predictions.  
22 *Hydrological Processes*. **17**, 887-900.
- 23 MacCormack, R.W., 1969. The effect of viscosity in hypervelocity impact cratering. *American*  
24 *Institute of Aeronautics and Astronautics*. Paper 69-354, New-York.
- 25 Mancilla, G.A.; Chen, S., McCool, D.K., 2005. Rill density prediction and flow velocity  
26 distributions on agricultural areas in the Pacific Northwest. *Soil & Tillage Research*, **84**(1),  
27 54-66.
- 28 Montgomery, D.R., Dietrich, W.E., 1992. Channels initiation and the problem of landscape  
29 scale. *Science*, **255**, 826-830.
- 30 Müller, E.N., 2004. Scaling approaches to the modelling of water, sediment and nutrient fluxes  
31 within semi-arid landscapes, Jornada Basin, New Mexico. Unpublished PhD thesis, King's  
32 College London, UK.
- 33 Nearing, M.A., Norton, L.D., Bulgakov, D.A., Larionov, G.A., West, L.T., Dontsova, K.M.,  
34 1997. Hydraulics and erosion in eroding rills. *Water Resources Research*, **33**, 865-876.
- 35 Nord, G., Esteves, M., 2005. PSEM\_2D: a physically-based model of erosion processes at the  
36 plot scale. *Water Resources Research*. **41**(8): Art. No. W08407.
- 37 Parsons, A.J. 1987. The role of slope and sediment characteristics in the initiation and  
38 development of rills. In Godard A and Rapp A. (eds) *Processus et mesure de l'érosion*,  
39 211-220, Editions du CNRS, Paris.
- 40 Parsons, A.J., Abrahams, A.D. and Wainwright, J. 1994. On determining resistance to interrill  
41 overland flow. *Water Resources Research*, **30**, 3515-3521.
- 42 Parsons, A.J., Wainwright, J., Abrahams, A.D., Simanton, J.R., 1997. Distributed dynamic  
43 modelling of interrill overland flow. *Hydrological Processes*, **11**(14), 1833-1859.

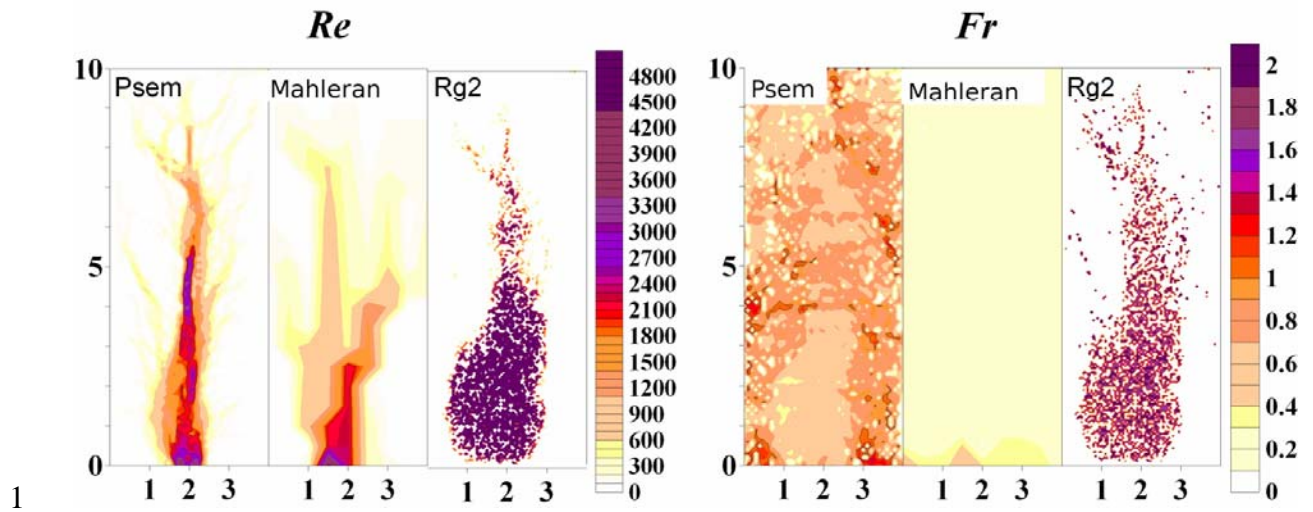
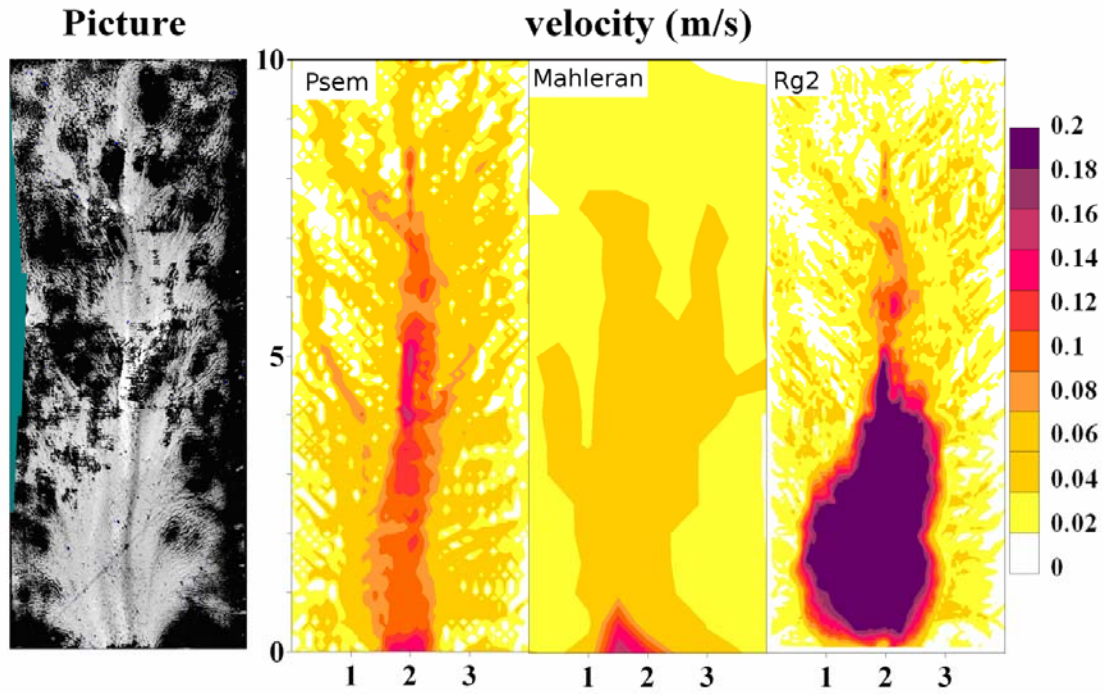
- 1 Patton P.C., Schumm S.A., 1975. Gully erosion, Northwest Colorado: a threshold  
2 phenomenon. *Geology*, **3**, 83-90.
- 3 Pilotti, M., Menduni, G., 1997. Application of lattice gas techniques to the study of sediment  
4 erosion and transport caused by laminar sheetflow. *Earth Surface Processes and*  
5 *Landforms*, **22**, 885-893.
- 6 Planchon, O., Darboux, F., 2001. A fast, simple and versatile algorithm to fill the depressions  
7 of digital elevation models. *Catena*, **46**(2-3), 159-176.
- 8 Planchon, O., Esteves, M., Silvera, N., Lapetite, J.M., 2001. Microrelief induced by tillage:  
9 measurement and modelling of Surface Storage Capacity. *Catena*, **46**(2-3), 141-157.
- 10 Planchon, O., Silvera, N., Gimenez, R., Favis-Mortlock, D., Wainwright, J., Lebissonais, Y.,  
11 Govers, G., 2005. Estimation of flow velocity in a rill using an automated salt-tracing  
12 gauge. *Earth Surface Processes and Landforms*, **30**, 833-844.
- 13 Rieke-Zap, D. H., Nearing M.A., 2005. Slope Shape Effects on Erosion: A Laboratory Study.  
14 *Soil Sciences Society of America Journal*, **69**(5), 1463-1471.
- 15 Roo, A.P.J. de, Wesseling, C.G., Ritsema, C.J., 1996. LISEM: a single event physically-based  
16 hydrologic and soil erosion model for drainage basins: I Theory, input and output.  
17 *Hydrological Processes*, **10**(8), 1107-1117.
- 18 Savat, J., 1980. Resistance to flow in rough supercritical sheet flow. *Earth Surface Processes*  
19 *and Landform*, **5**: 103-122.
- 20 Scoging, H., 1992. Modelling overland-flow hydrology for dynamic hydraulics. In: A. J.  
21 Parsons, A. D. Abrahams (Eds), *Overland Flow Hydraulics and Erosion Mechanics*..  
22 London, UCL Press, 89-103.
- 23 Song, W., Liu, P.L., Yang, M.Y., Xue, Y.Z., 2003. Using REE tracers to measure sheet erosion  
24 changing to rill erosion. *Journal of Rare Earths*, **21**(5), 587-590.
- 25 Thorne, C.R., Zevenbergen, L.W., 1990. Prediction of ephemeral gully erosion on cropland in  
26 the Southeastern. United States. In: J. Boardman, I.D.L. Foster, J.A. Dearing, Editors, *Soil*  
27 *Erosion on Agricultural Land*, Wiley, Chichester (1990): 447-460.
- 28 Vandaele, K., Poesen, J., Marques da Silva, J.R., Desmet, P., 1996. Rates and predictability of  
29 ephemeral gully erosion in two contrasting environments. *Geomorphology, Relief,*  
30 *Processes and Environment*, **2**, 83-96.
- 31 Wainwright, J., Parsons, A.J., Abrahams, A.D., 1999. Field and computer simulation  
32 experiments on the formation of desert pavement. *Earth Surface Processes and Landforms*,  
33 **24**, 1025-1037.
- 34 Wainwright, J., Parsons, A.J., 2002. The effect of temporal variations in rainfall on scale  
35 dependency in runoff coefficients. *Water Resources Research*, **38**(12), 1271. Doi:  
36 10.1029/2000WR000188.
- 37 Wainwright, J., Parsons, A.J., Müller, E.N., Brazier, R.E., Powell, D.M., Fenti, B., *in review*. A  
38 transport-distance approach to scaling erosion rates: model development and testing. *Earth*  
39 *Surface Processes and Landforms*.
- 40 Whiting, P.J.; Bonniwell, E.C.; Matisoff, G., 2001. Depth and areal extent of sheet and rill  
41 erosion based on radionuclides in soils and suspended sediment. *Geology*, **29**(12), 1131-  
42 1134.

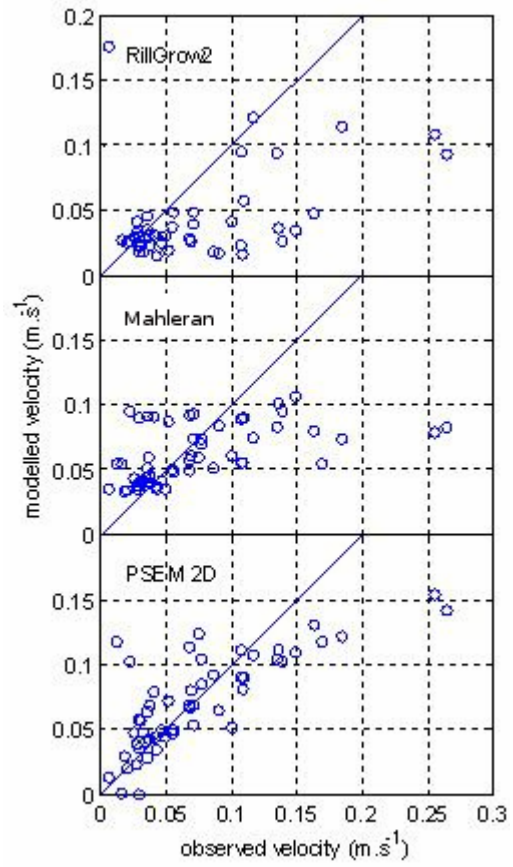
- 1 Yang, M.Y.; Walling, D.E.; Tian, J.L.; Liu, P.L., 2006. Partitioning the contributions of sheet
- 2 and rill erosion using beryllium-7 and cesium-137. *Soil Science Society of America Journal*,
- 3 **70**(5), 1579-1590
- 4 Zhang, W., Cundy, T. W., 1989. Modelling of two dimensional overland flows. *Water*
- 5 *Resources Research*, **25**, 2019-2035.

- 1 List of captions:  
2  
3 *Figure 1.* Location of the velocity measurements showed on a virtual picture of the plot.  
4 Vertical axis has been magnified ten times. Colour contrast has been enhanced. The native soil  
5 appears in black. White and reddish colours correspond to various types of sand deposits (see  
6 text for details).  
7  
8 *Figure 2.* Detail of the left bank of the rill viewed from downstream. Light blue crosses show  
9 velocity measurement locations. Coloured arrows are modelled flow velocity. Capital letters  
10 show the four surface features that develop on the plot (see comments in text). Axis labels are  
11 in mm.  
12  
13 *Figure 3.* Picture of the plot (with contrast magnified) compared to the velocity,  $Re$  and  $Fr$   
14 maps predicted by the three models. Calibrations based on the hydrograph.  
15  
16 *Figure 4.* Modelled velocity against measured values for the three models.  
17  
18 *Figure 5.* PSEM\_2D results with  $ff$  calculated from Eq. 14: output maps compared with the  
19 picture of the plot.  
20  
21 *Figure 6.* PSEM\_2D modelled velocity with  $ff$  calculated from Eq. 14.  
22  
23 *Figure 7.* Relationship between friction factor  $ff$  and Reynolds number  $Re$  simulated by  
24 PSEM\_2D with friction factor calculated from Eq. 14.  
25  
26 *Figure 8.* Relationship between Friction factor  $ff$  and Reynolds number  $Re$ : comparison with  
27 results from Nearing et al. (1997).  
28  
29  
30 *Table 1.* Qualitative information on flow conditions deduced from field observation during  
31 rainfall, and from surface-feature description after the experiment.

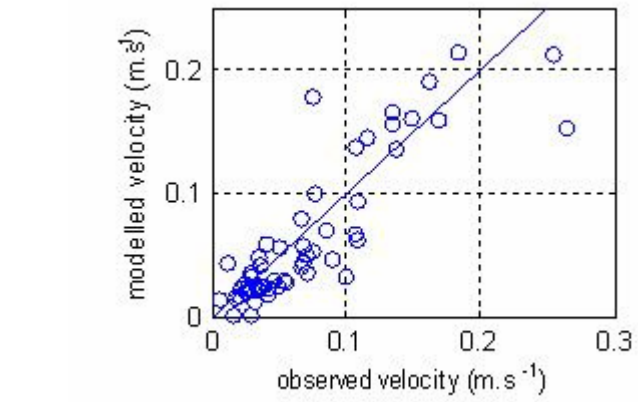
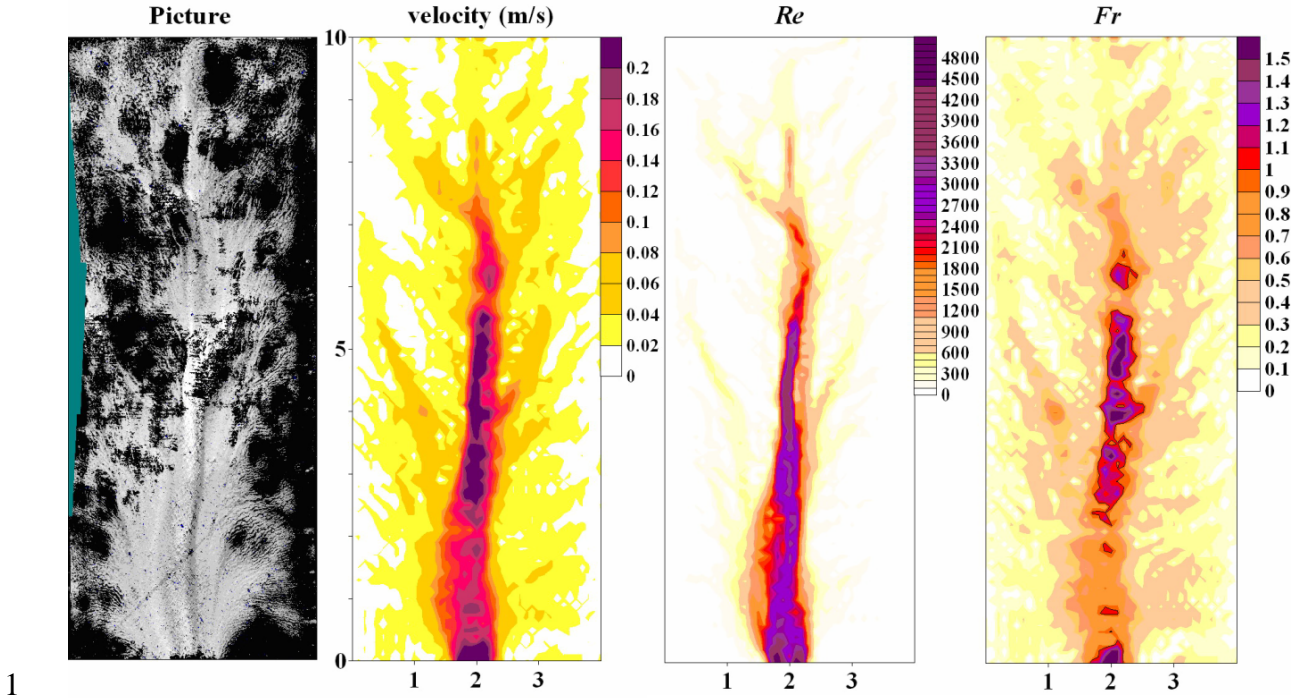


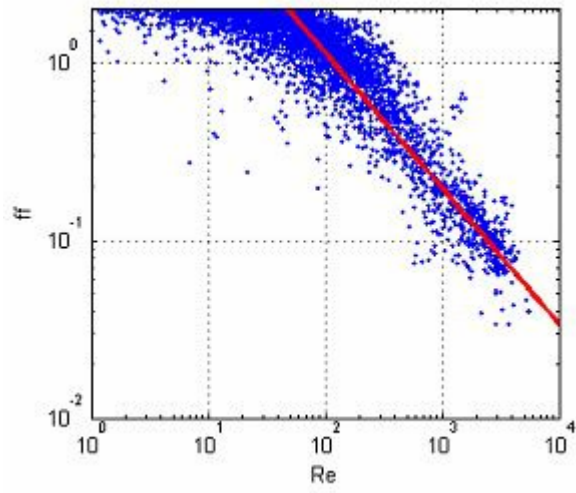




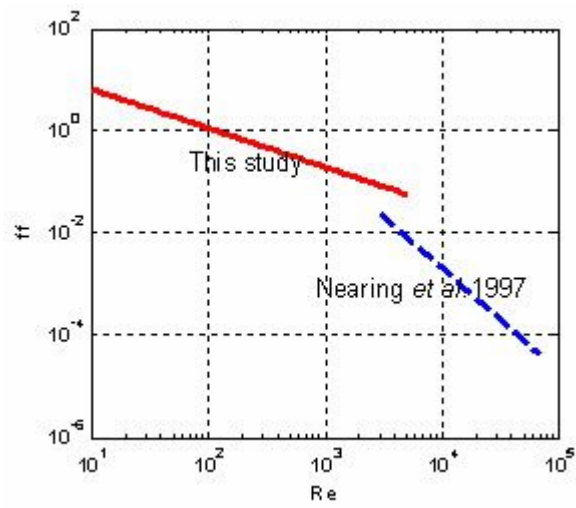


1





1



2

1

---

<b>Location</b>	<b>Surface feature from observation</b>	<b>Turbulence</b>	<b>Flow regime</b>
<i>A</i>	Native soil, light brown	Laminar, agitated by raindrop impacts	Subcritical
<i>B</i>	Discontinuous sand deposit		
<i>C</i>	Continuous reddish sand deposit	Turbulent	Supercritical
<i>D</i>	Continuous white sand deposit with crossed wavy features		

---

2

3 Table 1

4

5

6